Asian Journal of Chemistry; Vol. 38, No. 9 (2026), 2289-2300
ASIAN JOURNAL OF CHEMISTRY
https://doi.org/10.14233/ajchem.2026.36182

Design, Synthesis and *in vitro* Evaluation of Phthalimide-Anhydride Derivatives as MMP-9 Suppressors in Breast Cancer Therapy

SHITAL D. TIPLE[1], MANISHA P. PURANIK[1,*] and DEBARSHI KAR MAHAPATRA[2]

[1]Department of Quality Assurance, Institute of Pharmaceutical Education and Research, Borgaon (Meghe), Wardha-442001, India
[2]Chitkara College of Pharmacy, Chitkara University, Rajpura-140401, India

*Corresponding author: E-mail: manisha68_12@yahoo.com

Received: 20 May 2026 *Accepted*: 10 July 2026 *Published online*: 5 September 2026 AJC-22457

A novel series of substituted acetic 2-(1,3-dioxo-1,3-dihydro-2*H*-isoindol-2-yl)anhydride derivatives (**5a-e**) was designed and evaluated as potential matrix metalloproteinase-9 (MMP-9) suppressors for breast cancer therapy. Molecular docking using Schrödinger Maestro 2021 (PDB ID: 6ESM) revealed effective chelation of the catalytic Zn^{2+} ion by all derivatives, with the highest Glide score of -5.900 kcal/mol for compound **5a** and a promising -4.632 kcal/mol for lead candidate **5c** [acetic 2-(1,3-dioxo-1,3-dihydro-2*H*-isoindol-2-yl)-3-phenylpropanoic anhydride]. Molecular dynamics simulations confirmed the compound **5c**–MMP-9 complex stability (RMSD: 1.5-2.5 Å over 100 ns). SwissADME predictions indicated drug-like properties, including high gastrointestinal absorption, compliance with Lipinski's rule of five and no AMES mutagenicity or hERG inhibition. Compounds were synthesised *via* a two-step protocol involving phthalic anhydride condensation with amino acids followed by acetyl chloride-mediated cyclodehydration, affording yields of 46-65% (compound **5c**: 65%). *In vitro*, compound **5c** exhibited moderate cytotoxicity against MCF-7 breast cancer cells (IC_{50} = 27.89 μg/mL; 82.7 μM), approaching that of 5-fluorouracil (IC_{50} = 8.6 μg/mL; 66.1 μM) in the same assay system. Flow cytometry showed that compound **5c** induced early apoptosis (30.6% *vs.* 9.3% controls) and little necrosis. ELISA tests indicated that there was a concentration-dependent reduction of MMP-9 in TPA-stimulated MCF-7 cells (64.36% at a concentration of 55.89 μg/mL, 165.7 μM). Acute oral toxicity in rats gave an LD_{50} cut-off of 5-50 mg/kg (GHS Category 2), limiting the therapeutic window and requiring further optimisation before preclinical development. The phthalimide-anhydride scaffold offers a promising Zn^{2+}-chelating motif with potential selectivity over hydroxamates. Compound **5c** merits further lead optimisation, with *in vivo* efficacy, pharmacokinetics and selectivity against other MMPs requiring evaluation.

Keywords: MMP-9, Breast cancer, Phthalimide-anhydride, Molecular docking, ADMET, Molecular simulation.

INTRODUCTION

The isoindoline-1,3-dione (phthalimide) nucleus is a rigid, planar aromatic heterocycle that has attracted considerable interest because of its reported anticancer, anti-inflammatory and antimicrobial activities [1,2]. Its extended π-surface facilitates aromatic and hydrophobic interactions within enzyme binding sites, while the carbonyl groups can participate in hydrogen-bonding interactions. Furthermore, N-substitution provides a versatile means of tuning the steric environment, lipophilicity and molecular recognition properties of the scaffold. These distinctive structural and pharmacological features make phthalimide a valuable platform for the design and development of biologically active molecules.

MMP-9 (gelatinase B) is frequently overexpressed in breast cancer and associated with lymph node involvement, advanced tumor stage and poor prognosis [3,4]. By degrading the basement membrane components, particularly type-IV collagen, MMP-9 facilitates tumor invasion, angiogenesis and metastatic progression [5,6]. As the first-generation MMP inhibitors predominantly contained hydroxamate groups as Zn^{2+}-chelating motifs; however, their broad-spectrum activity and limited selectivity restricted their therapeutic potential [7,8]. These limitations have encouraged the development of selective, non-hydroxamate MMP-9 inhibitors targeting structural features such as the hydrophobic S1′ pocket and adjacent binding regions to improve Zn^{2+}-coordination and inhibitor selectivity [9,10].

The phthalimide-anhydride framework was designed by combining the rigid, planar aromatic phthalimide moiety with a carbonyl-rich anhydride functionality. The phthalimide core can facilitate hydrophobic and π-mediated interactions within the S1′ pocket of MMP-9, while the anhydride provides carbonyl oxygen atoms capable of interacting with the catalytic Zn^{2+} center. This architecture offers an alternative zinc-binding arrangement to conventional hydroxamate-based inhibitors and permits structural modulation through substitution of the phthalimide nitrogen and anhydride moieties [11,12]. Despite the pharmacological relevance of phthalimide derivatives, their systematic exploration as MMP-9 inhibitors remains limited.

In the present study, we report the design, synthesis and *in silico* and *in vitro* evaluation of novel acetic 2-(1,3-dioxo-1,3-dihydro-2H-isoindol-2-yl)anhydride derivatives as potential MMP-9 inhibitors. The hybrid scaffold was designed to combine the rigid aromatic surface of phthalimide for hydrophobic interactions within the MMP-9 binding pocket with the carbonyl-rich anhydride functionality for interaction with the catalytic Zn^{2+} center. Molecular docking and molecular dynamics simulations were employed to investigate binding interactions and complex stability, while ADMET profiling was used to assess drug-like properties. The synthesized compounds were further evaluated for cytotoxicity, apoptosis induction and MMP-9 suppression in MCF-7 breast cancer cells.

EXPERIMENTAL

All chemicals used in this study were of analytical grade and procured from reputable suppliers. 2-Benzofuran-1,3-dione (phthalic anhydride), amino-acetic acid (glycine), alanine, phenylalanine, leucine, valine, acetyl chloride and chloroform were obtained from Sigma-Aldrich (St. Louis, MO, USA). Solvents including glacial acetic acid, methanol and dimethyl sulfoxide (DMSO), were also sourced from Sigma-Aldrich. For *in vitro* studies, minimum essential medium (MEM) and Dulbecco's modified eagle medium (DMEM, Gibco, Invitrogen), fetal bovine serum (FBS, Gibco, Invitrogen) and antibiotic-antimycotic solution (Thermo-Fisher Scientific, Cat. No. 15240062) were used for cell culture. MTT reagent (Sigma-Aldrich), phosphate-buffered saline (PBS), trypsin-EDTA and sterile distilled water (HiMedia, India) were used for cell viability assays. 5-Fluorouracil (5-FU) and 12-O-tetradecanoylphorbol-13-acetate (TPA) were obtained from BLD Pharmatech (India) Pvt. Ltd. Apoptosis was assessed using the Annexin V–AbFluor™ 488 Apoptosis Detection Kit (Abbkine, China, Cat. No. KTA0002), while MMP-9 levels were quantified using the GENLISA™ Human MMP-9/Gelatinase B ELISA kit (Krishgen Biosystems, India; Cat. No. KBH0936, Ver. 6.3, RUO).

Instrumentation: Spectroscopic and analytical characterization of the synthesized compounds was performed using FTIR spectroscopy (IRTracer-100, Shimadzu), mass spectrometry (REIMS w/iKnife with HDI, Waters). ^{1}H NMR (400 MHz, Varian) and ^{13}C NMR (400 MHz, Agilent), with TMS as the internal standard. Elemental analyses were carried out using a Perkin-Elmer 2400 Series II analyzer. Thin-layer chromatography was performed on silica gel $60GF_{254}$ plates (Merck) and visualized under UV light at 254 nm. Melting points were determined by the open-capillary method without correction. For *in vitro* studies, a CO_2 incubator, Class II biosafety cabinet and ELISA plate reader were used. Flow cytometric analyses were performed using a Cytomics FC500 flow cytometer (Beckman Coulter) and FlowJo X software (v10.0.7).

Synthesis of phthalimide–acetic anhydride compounds (5a-e): Phthalimide-acetic anhydride compounds (**5a-e**) were synthesized by a two-step reaction [13,14]. The phthalimide-acetic acid intermediates (**3a-e**) were synthesized in step-1 by triturating equimolar amounts (0.01 mol each) of the corresponding amino acids and 2-benzofuran-1,3-dione (phthalic anhydride) in glacial acetic acid (10 mL). The reaction mixture was refluxed for 10 h and monitored by TLC using $CHCl_3$:EtOAc (1:1, v/v). After completion, the mixture was cooled and the resulting crystalline product was filtered, washed with cold water and recrystallized from methanol to afford intermediates **3a-e**. In step-2, the dried intermediates **3a-e** were refluxed with acetyl chloride for 1 h, with the reaction monitored by TLC using *n*-hexane:$CHCl_3$:EtOAc (4:1:1, v/v/v). After completion, the reaction mixture was cooled and poured into ice-cold water, yielding a white precipitate. The precipitate was filtered, washed thoroughly with water, dried in a desiccator and recrystallized from chloroform to obtain the corresponding anhydride derivatives **5a-e** in pure form (**Scheme-I**).

(1,3-Dioxo-1,3-dihydro-2*H*-isoindol-2-yl)acetic acid (3a): Off-white solid; yield 56%; R_f = 0.45 ($CHCl_3$:EtOAc, 1:1 v/v); m.p.: 153-156 ºC; FTIR (ATR, ν_{max}, cm^{-1}): 3566 (O-H, –COOH), 2989 (aliph. C–H), 1729 (C=O, imide/acid), 1605 (C=C, Ar), 1326 (C=O, imide), 715 (Ar–C–H, out-of-plane); ^{1}H NMR (500 MHz, DMSO-d_6, δ ppm): 13.3597 (br, s, 1H, –COOH), 7.8986-7.9387 (m, 2H, Ar-H), 7.8550-7.8986 (m, 2H, Ar-H), 4.2666-4.3257 (s, 2H, Gly-CH_2); ^{13}C NMR (125 MHz, DMSO-d_6, δ ppm): 168.08 (×1, C=O, COO^-), 166.61 (×2, C=O, imide), 130.78 (×2, Ar -Cq), 134.21 (×2, Ar-CH), 122.78 (×2, Ar-CH), 50.59 (×1, -CH_2); MS (ESI):

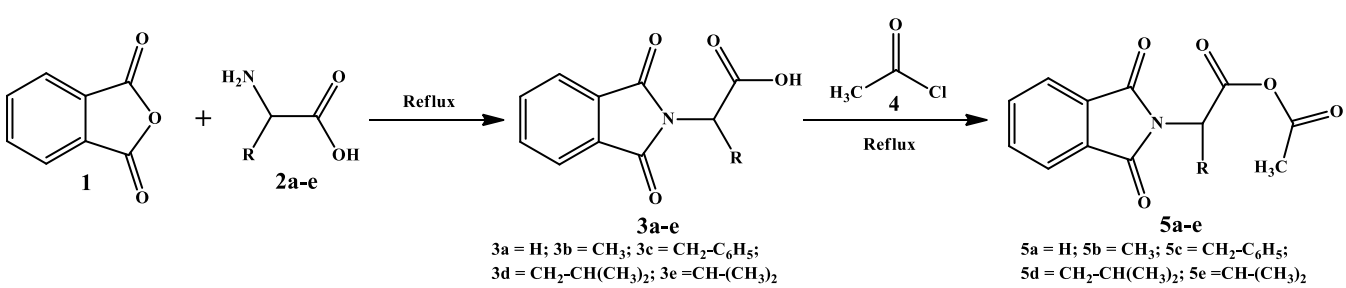

Scheme-I: Synthesis of substituted acetic 2-(1,3-dioxo-1,3-dihydro-2*H*-isoindol-2-yl) anhydride derivatives (**5a-e**)

m/z 205.01 $[M]^+$, 161.01 $[M\text{-}CO_2]^+$; Elemental analysis of $C_{10}H_7NO_4$: calcd (found) %: C, 58.54 (58.53); H, 3.44 (3.48); N, 6.83 (6.88).

2-(1,3-Dioxo-1,3-dihydro-2*H*-isoindol-2-yl)propanoic acid (3b): Off-white solid; yield 75%; R_f = 0.42 ($CHCl_3$: EtOAc, 1:1 v/v); m.p.: 103-104 ºC; FTIR (KBr, ν_{max}, cm^{-1}): 3220.90 (O-H); 3002.96 (=C–H *str*. arom.), 1778.25 (asym. C=O *str.*, imide), 1760.59 (sym. C=O *str.*, imide), 1680.87 (C=O *str.*, -COOH); ^{1}H NMR (500 MHz, DMSO-d_6, δ ppm): 13.1248 (br, s, 1H, CO_2H), 7.8561-7.8879 (m, 2H, Ar-H), 7.8201-7.8521 (m, 2H, Ar-H), 4.8575-4.9014 (q, 1H, *J* = 7.3 Hz, Ala –CH), 1.5652-1.5799 (d, 3H, *J* = 7.3 Hz, Ala-CH_3); ^{13}C NMR (125 MHz, DMSO-d_6, δ ppm): 171.07 (CO_2H, C=O); 167.14 × 2 (2 C, imide, C=O), 131.30× 2 (2C, Ar-C), 123.21 × 2 (2C, Ar–CH), 134.63 × 2 (2C, Ar-CH); 47.02 (-CH, αC of Ala), 14.82 (-CH_3, methyl of Ala); MS (ESI): *m/z* 218.91 $[M\text{-}1]^+$, 175.01 $[M\text{-}CO_2]^+$, 160.01 $[M\text{-}C_2H_3O_2]^+$; Elemental analysis of $C_{11}H_9NO_4$: calcd. (found) %: C, 60.27 (60.24); H, 4.14 (4.18); N, 6.39 (6.38).

2-(1,3-Dioxo-1,3-dihydro-2*H*-isoindol-2-yl)-3-phenylpropanoic acid (3c): Off-white solid; yield 82%; R_f = 0.39 ($CHCl_3$:EtOAc, 1:1 v/v); m.p.: 155-156 ºC; FTIR (KBr, ν_{max}, cm^{-1}): 3280-3200 (br, O–H *str*., –COOH), 3050-3010 (Ar-C–H *str*.), 1760, 1705 (C=O *str.*, imide), 1718 (C=O *str*., -COOH), 760, 720 (C–H oop, mono-substituted Ar ring); ^{1}H NMR (500 MHz, DMSO-d_6, δ ppm): 13.3966 (br, s, 1H, CO_2H), 7.7761-7.8263 (m, 4H, Ar-H, phthalimide), 7.0797-7.1663 (m, 5H, Ar-H, phenyl), 5.1468-5.1798 (q, 1H, *J* = 5.5 Hz, α-CH), 3.5054-3.5432 (dd, 1H, *J* = 6.3 Hz, β-CH_2), 3.3696-3.4213 (dd, 1H, *J* = 8.6 Hz, β-CH_2); ^{13}C NMR (125 MHz, DMSO-d_6, ppm): 170.08 (C=O, -COOH), 167.08 × 2 (2C, C=O, imide); 137.28, 130.70 × 2 (3C, Ar-C), 123.36 × 2, 126.58 × 1, 128.32 × 2, 128.74 × 2, 134.86 × 2 (9C, Ar -CH), 33.94 (-CH_2, β-carbon), 52.92 (-CH, α-carbon); MS (ESI) *m/z* 294 $[M\text{-}1]^+$, 278.9 $[M\text{-}OH]^+$, 250.0 $[M\text{-}COOH]^+$, 159 $[M\text{-}C_8H_8O_2]^+$ base peak, 148 $[M\text{-}C_9H_9O_2]^+$; Elemental analysis of $C_{17}H_{13}NO_4$: calcd. (found) %: C, 69.15 (69.13); H, 4.44 (4.48); N, 4.74 (4.78).

2-(1,3-Dioxo-1,3-dihydro-2*H*-isoindol-2-yl)-4-methylpentanoic acid (3d): Off-white solid; yield 60%; R_f = 0.49 ($CHCl_3$:EtOAc, 1:1 v/v); m.p.: 105-108 ºC; FTIR (KBr, ν_{max}, cm^{-1}): 3200-2800 (br, O–H *str*., -COOH), ~1725 (C=O *str.*, -COOH), ~1705 (-C=O *str.*, imide); ^{1}H NMR (500 MHz, DMSO-d_6, δ ppm): 13.1942 (br, s, 1H, -COOH), 7.8849-7.9169 (m, 2H, Ar-H), 7.8488-7.8739 (m, 2H, Ar-H), 4.7781-4.8097 (m, 1H, Leu-CH), 1.8310-1.8881, 2.1579-2.2173 (m, 2H, Leu-CH_2), 1.4018-1.4566 (m, 1H, Leu-CH), 0.8336-0.8683 (dd, 6H, Leu-$(CH_3)_2$); ^{13}C NMR (125 MHz, DMSO-d_6, δ ppm): 170.798 (C=O, -COOH), 167.40 × 2 (C=O, imide), 131.07 × 2 (-C, Ar-Cq), 123.32 × 2, 134.75 × 2 (Ar-CH), 50.08 (-CH, Leu), 36.68 (-CH_2, Leu), 24.59 (-CH, Leu), 20.72, 22.91 (-CH_3, Leu); MS (ESI): *m/z* 261.01 $[M]^+$, 217.00 $[M\text{-}CO_2]^+$, 160.01 $[(M–(CO_2+C_4H_9)]^+$; Elemental analysis of $C_{14}H_{15}NO_4$: calcd (found) %: C, 64.36 (64.30); H, 5.79 (5.68); N, 5.36 (5.37).

2-(1,3-Dioxo-1,3-dihydro-2*H*-isoindol-2-yl)-3-methylbutanoic acid (3e): Off-white solid; yield 74%; R_f = 0.63 ($CHCl_3$:EtOAc, 1:1 v/v); m.p.: 102-104 ºC; FTIR (KBr, ν_{max}, cm^{-1}): 3300-2500 (br, O–H *str*., -COOH), 2960-2850 (C-H *str*. alkyl), 1680-1720 (C=O *str*., -COOH), 1800-1760 (-C=O *str*. sym. and -C=O *str*. asym., imide); ^{1}H NMR (500 MHz, DMSO-d_6, δ ppm): 13.0161 (br, s, 1H, CO_2H), 7.8923-7.9173 (m, 2H, Ar-H), 7.8540-7.8791 (m, 2H, Ar-H), 4.4515-4.4673 (d, 1H, *J* = 7.9 Hz, α-CH), 2.5448-2.6144 (sextet, 1H, *J* = 6.96 Hz, -CH), 1.0589-1.0722 (d, 3H, *J* = 6.65 Hz, -CH_3), 0.8128-0.8265 (d, 3H, *J* = 6.85 Hz, -CH_3); ^{13}C NMR (125 MHz, DMSO-d_6, δ ppm): 169.75 (C=O, CO_2H), 167.43 × 2 (C=O, imide carbonyls), 130.95 × 2 (-Cq, Ar), 123.42 × 2, 134.85 × 2 (-CH, Ar), 56.99 (-CH, α-carbon next to CO & CH), 27.98 (-CH, tertiary carbon bearing 2× -CH_3), 20.85 (-CH_3), 19.24 (-CH_3); MS (ESI): *m/z* 246.91 $[M]^+$, 203.01 $[M\text{-}CO_2]^+$, 159.91 $[M\text{-}C_4H_7O_2]^+$; Elemental analysis of $C_{13}H_{13}NO_4$: calcd. (found) %: C, 63.15 (63.10); H, 5.30 (5.29); N, 5.67 (5.67).

Acetic (1,3-dioxo-1,3-dihydro-2*H*-isoindol-2-yl)acetic anhydride (5a): White solid; yield 50%; R_f = 0.45 (*n*-hexane: $CHCl_3$:EtOAc, 4:1:1 v/v/v); m.p.: 147-149 ºC; IR (ATR, ν_{max}, cm^{-1}): 1771, 1711 (C=O, anhydride/imide), 1604-1390 (Ar C=C, CH_2/CH bending), 1338-1211 (C–O–C *str.*), 1121-1010 (C-O/C-N), 954 (anhydride *def.*), 891-714 (Ar C-H, oop); ^{1}H NMR ($CDCl_3$, 400 MHz, δ ppm): 3.71 (3H, s, CH_3CO-), 4.72 (2H, s, -CH_2–CO-), 7.746-7.767 (dd, *J* = 5.40, 3.0 Hz, 2H, Ar–H), 7.888-7.909 (dd, *J* = 5.40, 3.0 Hz, 2H, Ar–H); ^{13}C NMR ($CDCl_3$, 100 MHz, δ ppm): 20.9 (-CH_3), 42.2 (-CH_2), 123.8 ×2, 134.7 ×2 (Ar-CH), 131.9 ×2 (Ar-C), 167.6, 168.0, 171.7 (C=O); MS (ESI, *m/z*): 247 (M^+), 186 $[C_{10}H_4NO_3^+]$, 160 $[C_9H_6NO_2^+]$, 134 $[C_8H_8NO^+]$, 132 $[C_9H_8O^+]$, 105 $[C_7H_5O^+]$. Anal. analysis of $C_{12}H_9NO_5$: calcd. (found) %: C, 58.30 (59.00); H, 3.67 (3.68); N, 5.67 (5.68).

Acetic 2-(1,3-dioxo-1,3-dihydro-2*H*-isoindol-2-yl)propanoic anhydride (5b): White solid; yield 46%; R_f = 0.54 (*n*-hexane:$CHCl_3$:EtOAc, 4:1:1 v/v/v); m.p.: 95-97 ºC; FTIR (ATR, ν_{max}, cm^{-1}): 3009 (Ar–C–H), 2972, 2868, 2844 (aliph. C–H), 1846, 1793 (anhydride C=O), 1760 (acetyl C=O), 1669 (imide C=O), 1584-1524 (Ar C=C), 1469, 1400, 1358-1335 (C–H/C–N), 1256 (C–O–C), 1158-1055, 1027-1010 (C–O/C–C), 900-710 (Ar C–H oop); ^{1}H NMR (400 MHz, $CDCl_3$, ppm): 7.912-7.934 (dd, *J* = 5.6, 2.2 Hz, 2H, Ar-H), 8.029-8.051 (dd, *J* = 5.6, 3.2 Hz, 2H, Ar-H), 5.12 (q, *J* = 7.0 Hz, 1H, CH–), 2.24 (s, 3H, O=C–CH_3), 1.53 (d, *J* = 7.0 Hz, 3H, CH-CH_3); ^{13}C NMR (100 MHz, $CDCl_3$, δ ppm): 15.2 (1C, s) 20.9 (1C, s), 47.3 (1C, s), 123.8 (2C, s), 124.7 (2C, s), 131.7 (2C, s), 167.8 (2C, s), 168.0 (1C, s) 168.4 (1C, s); MS (ESI, *m/z*): 261 $[M^+]$, 174 $[C_{10}H_8NO_2^+]$, 172 $[C_{10}H_6NO_2^+]$, 171 $[C_{10}H_5NO_2^+]$, 133 $[C_8H_5O_2^+]$, 107 $[C_7H_7O^+]$, 105 $[C_7H_5O^+]$. Anal. analysis of $C_{13}H_{11}NO_5$: calcd. (found) %: C, 58.30 (59.00); H, 3.67 (3.68); N, 5.67 (5.68).

Acetic 2-(1,3-Dioxo-1,3-dihydro-2*H*-isoindol-2-yl)-3-phenylpropanoic anhydride (5c): White solid; yield 65%; R_f = 0.48 (*n*-hexane:$CHCl_3$:EtOAc, 4:1:1 v/v/v); m.p.: 145-148 ºC; IR (ATR, ν_{max}, cm^{-1}): 2972-2820 (aliph. C–H), 1768, 1742 (anhydride C=O), 1692 (imide C=O), 1607 (C=C, Ar), 1256-1173 (C–O), 720, 700 (Ar–H, oop); ^{1}H NMR (400 MHz, $CDCl_3$, δ ppm): 2.10 (s, 3H, CH_3), 3.58-3.60 (d, *J* = 8.8 Hz, 2H, CH_2–Ph; diastereotopic, overlapped), 5.206-5.225 (t, *J* = 8.4 Hz, 1H, CH-α), 7.12-7.21 (m, 5H, Ar-H, phenyl), 7.67-7.68 (dd, *J* = 5.6, 3.2 Hz, 2H, Ar-H, isoindole), 7.75-7.78 (dd, *J* = 6.4, 3.2 Hz, 2H, Ar-H, isoindole); ^{13}C NMR (100 MHz, $CDCl_3$,

δ ppm): 20.9 (CH_3), 35.7 (CH_2), 51.2 (CH), 123.5 (2C, Ar-CH), 126.9 (Ar-CH), 128.5 (2C, Ar-CH), 128.7 (2C, Ar-CH), 134.1 (2C, Ar-CH), 131.3 (2C, Ar-Cq), 136.3 (Ar-Cq), 167.4 (2C, C=O, imide), 171.0 (2C, C=O, anhydride); MS (ESI, *m/z*): 337 $[M]^+$, 172 $[C_{10}H_6NO_2^+]$, 171 $[C_{10}H_5NO_2^+]$, 105 $[C_7H_5O^+]$. Anal. analysis of $C_{19}H_{15}NO_5$: calcd. (found) % C, 67.65 (68.36); H, 4.48 (4.82); N, 4.15 (4.59).

Acetic 2-(1,3-dioxo-1,3-dihydro-2*H*-isoindol-2-yl)-4-methylpentanoic anhydride (5d): White solid; yield 60%; R_f = 0.57 (*n*-hexane:$CHCl_3$:EtOAc, 4:1:1 v/v/v); m.p.: 103–105 ºC. FTIR (ATR, ν_{max}, cm^{-1}): 2965-2825 (aliphatic C–H *str.*), 1778 (imide C=O asym. *str.*), 1709 (imide/anhydride C=O sym. *str.*), 1611 (arom. C=C *str.*); ^{1}H NMR (400 MHz, $CDCl_3$, δ ppm): 7.841-7.881 (2H, m, Ar-H), 7.715-7.736 (2H, m, Ar-H), 4.981-5.021 (1H, m, N-CH), 2.334-2.409 (1H, m, CH_2-α, diastereotopic), 2.10 (3H, s, $OCOCH_3$), 1.92-1.99 (1H, m, CH), 1.463-1.532 (1H, m, CH_2-β, diastereotopic), 0.92-0.96 (6H, d, 2 × CH_3, isopropyl); ^{13}C NMR (100 MHz, $CDCl_3$, δ ppm): 168.4, 168.0 (2C, -C=O, anhydride), 167.8 (2C, -C=O, imide), 131.7 (2C, Ar-Cq), 124.7 (2C, Ar-CH), 123.8 (2C, Ar-CH), 51.2 (-CH), 36.6 (-CH_2), 25.0 (-CH), 22.5 (2× CH_3); MS (ESI, *m/z*): 303 $[M]^+$, 212 $[C_{13}H_{10}NO_2]^+$; Anal. analysis of $C_{16}H_{17}NO_5$: calcd. (found) %: C, 63.36 (63.36); H, 5.65 (5.82); N, 4.62 (4.69).

Acetic 2-(1, 3-dioxo-1,3-dihydro-2*H*-isoindol-2-yl)-3-methylbutanoic anhydride (5e): White solid; yield 60%; R_f = 0.74 (*n*-hexane:$CHCl_3$:EtOAc, 4:1:1 v/v/v); m.p.: 97-99 ºC. FTIR (ATR, ν_{max}, cm^{-1}): 2965-2826 (aliph. C-H), 1763 (C=O, anhydride), 1690 (C=O, imide), 1609 (C=C, aromatic), 966-901 (arom. C-H bending), 835-722 (arom. C-H, oop *bend.*); ^{1}H NMR ($CDCl_3$, 400 MHz, δ ppm): 2.733-2.788 (1H, sextet, $J \approx 7.3$ Hz, -CH adjacent to $(CH_3)_2$), 0.913-0.930 (3H, d, J = 6.8 Hz, CH_3), 1.161-1.177 (3H, d, J = 6.4 Hz, CH_3), 2.105 (3H, s, CH_3CO), 4.622-4.643 (1H, d, J = 8.4 Hz, -CH), 7.736-7.767(2H, dd, J = 4.0, 3.2 Hz, Ar-H), 7.854-7.884 (2H, dd, J =4.0, 2.8 Hz, Ar-H); ^{13}C NMR ($CDCl_3$, 100 MHz, δ ppm): 19.3-19.4 (2C, CH_3), 20.9 (1C, CH_3), 30.8 (1C, CH), 56.6 (1C, CH), 123.8 (2C, Ar-CH), 124.7 (2C, Ar-CH), 131.7 (2C, Ar-Cq), 167.8 (2C, C=O, imide), 168.0 (1C, C=O, anhydride), 168.4 (1C, C=O, anhydride); MS (ESI, *m/z*): 289 $[M]^+$, 228 $[C_{13}H_{10}NO_3]^+$, 203$[C_{12}H_{13}NO_2^+]$, 160 $[C_9H_6NO_2^+]$, 105 $[C_7H_5O^+]$; Anal. analysis of $C_{15}H_{15}NO_5$: calcd. (found) %: C, 62.28 (62.36); H, 5.23 (5.22); N, 4.84 (4.89).

In silico studies

Molecular docking: The binding interactions of the designed substituted acetic 2-(1,3-dioxo-1,3-dihydro-2*H*-isoindol-2-yl) anhydride derivatives (**5a-e**) with matrix metalloproteinase-9 (MMP-9) were investigated using molecular docking studies performed with the Glide module of the Schrödinger Maestro software suite.

Protein preparation: The crystal structure of MMP-9 was retrieved from the RCSB Protein Data Bank (PDB ID: 6ESM; 1.65 Å resolution). The structure was selected since it contains the complete catalytic domain, the catalytic Zn^{2+} ion and key active-site residues, His226, His230 and Glu402, involved in metal coordination and ligand recognition. Protein preparation was performed using the Protein Preparation Wizard in Schrödinger Maestro. Missing hydrogen atoms and bond orders were assigned, followed by optimization of the hydrogen bonding network and assignment of protonation states and tautomers of ionizable residues at pH 7.4. His226 and His230 were treated in their neutral states, while Asp185 and Glu402 were maintained in their deprotonated forms.

The catalytic Zn^{2+} ion and relevant heteroatoms were retained during preparation, with Zn^{2+} parameters assigned using the OPLS4e force field. Water molecules located beyond 5 Å from the active site were removed. The active site was defined by the Zn^{2+} ion and residues within 5 Å, namely His226, His230, Glu402, Tyr240 and Leu188. Four conserved water molecules (Wat501-Wat504), located within 3 Å of Zn^{2+} and involved in interactions with the coordinating residues, were retained to preserve the local hydration environment and ligand-binding architecture of the catalytic site, consistent with reported MMP-9 structural studies [15,16]. The prepared protein structure was energy-minimized using the OPLS4e force field until convergence, with a heavy-atom RMSD threshold of 0.3 Å.

Ligand preparation: Ligand structures for **5a-e** were initially drawn in ChemDraw Professional v21.0 (Perkin-Elmer Informatics, Waltham, USA) and imported into the Schrödinger environment. Three-dimensional conformers were generated using the LigPrep module, which applied the OPLS4e force field for geometry optimisation and enumerated relevant ionisation and tautomeric states at pH 7.4 ± 0.4 to match physiological conditions and avoid non-physiological anhydride protonation (excluding hydrolysed open-chain forms). The Epik module was used to predict the predominant protonation states of the ligands, with the neutral anhydride form selected for Zn^{2+}-binding studies. The effect of imide tautomerism was assessed by docking both keto and enol forms. The keto form was favoured, with an energy difference of <1 kcal/mol and docking-score variations of approximately 0.5 kcal/mol across the series, supporting the stability of the selected tautomeric state [17]. Up to 32 low-energy conformers were retained for each ligand. Stereoisomeric forms were generated for the chiral centers of compounds **5b-e**, consistent with their derivation from L-amino acid precursors.

Docking protocol: Molecular docking was performed using Glide in standard precision (SP) mode to generate initial ligand poses. Protein side chains within 5 Å of each ligand were refined using Prime, followed by extra-precision (XP) Glide docking of the refined complexes. Glide scores were recorded in kcal/mol and used as a comparative measure of ligand binding, with more negative values representing stronger predicted binding. Ligand–protein interactions were analyzed using the Maestro Interaction Diagram tool, with particular attention to hydrogen bonding with Gln227 and Tyr240, hydrophobic contacts within the S1′ and S2′ subsites and interactions with the catalytic Zn^{2+} ion. Two-dimensional interaction maps and three-dimensional docking poses were examined to assess ligand orientation and the involvement of key active-site residues in MMP-9 recognition [18].

Molecular dynamics (MD) simulations: Molecular dynamics (MD) simulation was performed for the **5c**–MMP-9 complex using the Desmond package [19]. Compound **5c** was selected based on its favourable docking score (-4.632 kcal/mol) and cytotoxic activity against MCF-7 breast cancer cells

(IC_{50} = 27.89 μg/mL). The complex was solvated in a 10 Å × 10 Å × 10 Å orthorhombic simulation box using SPC water. Na^+ or Cl^- ions were added to neutralize the system. The solvated system was energy-minimized using the OPLS3e force field. Steepest-descent minimization was followed by conjugate-gradient minimization until the gradient reached <0.1 kcal/mol. The production run was performed in the NPT ensemble at 300 K and 1.01325 bar using a Nose-Hoover chain thermostat for temperature regulation and a Martyna-Tobias-Klein barostat for pressure control. The simulation was conducted for 100 ns with a 2 fs integration time step and trajectory frames were recorded at 100 ps intervals. Trajectory analysis was performed using the Simulation Interaction Diagram (SID) tool in Desmond. Protein–ligand complex stability was assessed from the root-mean-square deviation (RMSD), residue flexibility from the root-mean-square fluctuation (RMSF) and ligand recognition from the protein-ligand interaction profile [20].

ADMET prediction: The ADMET profiles of synthesized compounds **5a-e** were evaluated using the SwissADME web tool [21]. Gastrointestinal (GI) absorption, blood-brain barrier permeability, P-glycoprotein substrate status, P450 inhibition, cytochrome and Lipinski's rule of five were assessed to estimate their drug-likeness and pharmacokinetic properties. AMES mutagenicity and hERG inhibition were examined as toxicity-related parameters. Compounds with favourable GI absorption and pharmacokinetic profiles were prioritized for subsequent *in vitro* evaluation.

In vitro studies

Cell line and culture: Human MCF-7 breast cancer cells were procured from the National Centre for Cell Science (NCCS, Pune, India). Cells were cultured in minimum essential medium (MEM) supplemented with 10% fetal bovine serum (FBS) and 1× antibiotic-antimycotic solution. Cultures were maintained at 37 ± 1 ºC in a humidified 5% CO_2 incubator. For apoptosis assays, cells were cultured in DMEM (low glucose) with the same supplements. All cell culture procedures were performed in a Class II biosafety cabinet to ensure sterility.

MTT assay: The MTT assay was conducted to determine the cytotoxic activity of the synthesised compounds against the MCF-7 cells. Cells were plated at a density of 1 × 10^4 cells/well in 96-well plates and incubated for 24 h at 37±1 ºC under 5% CO_2. The test compounds were dissolved in DMSO (final concentration of 0.2%) and then diluted in culture medium to vary their concentration from 12.5 to 100 μg/mL. Control wells were treated with 0.2% DMSO in PBS. Following treatment for 24 h, the medium was discarded and 20 μL of MTT solution (5 mg/mL in PBS) was added to each well. The plates were allowed to incubate for over 4 h in the sufficiency of 37 ± 1 ºC, such that crystals of formazan could develop. Aspiration of the supernatant and the addition of 200 μL of DMSO to both wells to dissolve the formazan were performed. The plates were left to incubate (10 min) at room temperature (37 ± 1.0 ºC) in darkness and the absorbance of the plates at 570 nm was measured using an ELISA plate reader. The viability of cells was computed against the control and the IC_{50} were obtained based on the dose-response curves [22]. Each experiment was conducted in triplicate.

Apoptosis assay: Apoptosis induced by compound **5c** in MCF-7 cells was evaluated using the AbFluor™ 488 Annexin V Apoptosis Detection Kit. Cells were seeded in six-well plates at 1 × 10^6 cells/mL and incubated overnight at 37 ± 1 ºC in a humidified 5% CO_2 atmosphere. Cells were treated with **5c** (30 μg/mL; 88.93 μM) for 24 h, washed twice with PBS and centrifuged at 500 × g for 5 min at 4 ± 1 ºC. The resulting pellets were resuspended in ice-cold 1× Annexin V binding buffer (0.1 M HEPES/NaOH, pH 7.4; 1.4 M NaCl; 25 mM $CaCl_2$) at 1 × 10^6 cells/mL. For staining, 5 μL of AbFluor™ 488 Annexin V and 2 μL of propidium iodide (PI) were added to each sample. The samples were incubated for 15 min at room temperature in the dark, followed by addition of approximately 400 μL of ice-cold binding buffer. Flow-cytometric analysis was performed within 30 min using a Cytomics FC500 flow cytometer. Data were analyzed with FlowJo X software (version 10.0.7) to quantify viable, early apoptotic, late apoptotic and necrotic cell populations [23].

MMP-9 quantification by ELISA: The effect of compound **5c** on TPA-induced MMP-9 secretion in MCF-7 breast cancer cells was evaluated using the GENLISA™ Human MMP-9 ELISA kit. Untreated cells served as the basal control, while TPA-treated cells served as the MMP-9 induction control. Compound **5c** was tested at ½IC_{50} (13.94 μg/mL; 41.3 μM), IC_{50} (27.89 μg/mL; 82.7 μM) and 2×UC_{50} (55.89 μg/mL; 165.7 μM), based on the MTT assay. 5-Fluorouracil (5-FU) was used as the reference drug at 5, 10 and 20 μM (0.650, 1.3008 and 2.6016 μg/mL, respectively). MCF-7 cells were seeded in 12-well plates at 8 × 10^4 cells/mL and incubated for 20 h at 37 ± 1 ºC under 5% CO_2. The cells were washed with PBS and maintained in serum-free medium for 4 h. Cells were pretreated with compound **5c** at the selected concentrations for 1 h, followed by treatment with TPA (0.1 μM) to induce MMP-9 secretion. Untreated and TPA-only groups served as negative and positive controls, respectively. After 24 h, culture supernatants were collected and centrifuged at 1000 × g for 10 min to remove cellular debris. For ELISA, 100 μL of standards and samples were added to the pre-coated wells and incubated for 90 min at 37 ± 1 ºC. The wells were washed three times with 1× wash buffer, followed by addition of 100 μL biotinylated anti-MMP-9 antibody and incubation for 60 min. After washing, 100 μL streptavidin-HRP conjugate was added and incubated for 30 min. The wells were washed again, followed by addition of 100 μL TMB substrate and incubation for 15 min in dark. The reaction was stopped with 100 μL stop solution and absorbance was measured at 450 nm using a microplate reader. MMP-9 concentrations were calculated from the corresponding standard curve according to the manufacturer's protocol [24].

Acute oral toxicity study: Acute oral toxicity of compound **5c** was evaluated in female albino Wistar rats (n = 3) according to OECD Guideline 423 under approved protocol no. 535/PO/ReReBt/S/02/CPCSEA/IPER/IAEC/2024-25/32. Animals were fasted overnight with free access to water before oral administration of **5c** at sequential doses of 300, 50 and 5 mg/kg body weight, using the OECD-recommended dose progression. Animals were monitored continuously for the first 4 h, at regular intervals during the first 24 h and daily

for 14 days for mortality, behavioral changes and clinical signs of toxicity. Dose progression was adjusted according to mortality at each dose level. The LD_{50} cut-off was assigned from the observed mortality pattern according to OECD Guideline 423 [25].

RESULTS AND DISCUSSION

The target phthalimide-anhydride derivatives (**5a-e**) were synthesized through a two-step route involving the corresponding phthalimide-acetic acid intermediates (**3a-e**). Phthalic anhydride was reacted with glycine, alanine, phenylalanine, leucine or valine in glacial acetic acid. The reaction was monitored by TLC using $CHCl_3$/EtOAc (1:1, v/v). The reaction conditions were dependend on the amino acid substituent. Solid-state fusion at 100 ± 1 ºC gave the glycine-derived intermediate **3a** in 36% yield. The substituted amino acids required reflux in glacial acetic acid for 10 h, giving **3b** (75%), **3c** (82%), **3d** (60%) and **3e** (74%). Then, cyclodehydration of intermediates **3a-e** afforded the corresponding anhydrides **5a-e** using acetyl chloride under reflux for 1 h. TLC was performed using *n*-hexane/$CHCl_3$/EtOAc (4:1:1, v/v/v). Acetic anhydride in the presence of $ZnCl_2$ did not afford complete conversion, with starting-material spots remaining on the TLC plates. Acetyl chloride gave the desired products as white solids after recrystallization from chloroform. The highest yield obtained for compound **5c** corresponds to the favourable yield of its precursor **3c**. The higher electrophilic character of acetyl chloride provides a plausible explanation for its superior performance in the cyclodehydration step compared with acetic anhydride under the conditions investigated [14].

The synthesized intermediates and final compounds were characterized by FTIR, ^{1}H NMR, ^{13}C NMR, ESI-MS and elemental analysis. Intermediate **3a** displayed O–H, aliphatic C–H and carbonyl absorptions at 3566, 2989 and 1729 cm^{-1}, respectively. Its ^{1}H NMR spectrum contained a COOH signal at δ 13.36 ppm and a CH_2 singlet at δ 4.27 ppm. Intermediate **3c** showed a broad O–H absorption at 3280-3200 cm^{-1} and aromatic C–H absorptions at 3050-3010 cm^{-1}, with aromatic protons at δ 7.08-7.17 ppm. Conversion to the anhydrides was supported by the appearance of characteristic anhydride carbonyl bands. Compound **5a** showed absorptions at 1771 and 1711 cm^{-1} and a CH_3CO signal at δ 3.71 ppm in the ^{1}H NMR spectrum. Compound **5c** displayed anhydride carbonyl bands at 1768 and 1742 cm^{-1} and an aromatic C=C band at 1607 cm^{-1}. Its ^{1}H NMR spectrum showed phenyl protons at δ 7.12-7.21 ppm and diastereotopic CH_2 protons at δ 3.58-3.60 ppm.

In silico studies

Molecular docking: Molecular docking was performed to examine the binding of substituted acetic 2-(1,3-dioxo-1,3-dihydro-2H-isoindol-2-yl) anhydride derivatives (**5a-e**) within the MMP-9 catalytic region using the Schrödinger Maestro 2021 suite, Glide and the Induced Fit Docking (IFD) protocol. The MMP-9 crystal structure 6ESM was selected for its high structural resolution and well-defined catalytic region. The deposited 6ESM structure has a resolution of 1.10 Å and contains the E402Q variant; this residue assignment should be retained in the docking description unless Gln402 was explicitly reverted to Glu402 during protein preparation. The docking scores ranged from -3.685 to -5.900 kcal/mol (Table-1), providing a comparative measure of the predicted binding of the synthesized derivatives.

TABLE-1
MOLECULAR DOCKING SCORE OF SUBSTITUTED ACETIC 2-(1,3-DIOXO-1,3-DIHYDRO-2*H*-ISOINDOL-2-YL) ANHYDRIDE DERIVATIVES (**5a-e**)

Compound	Docking score	Interaction with amino acids	Others
5a	-5.9	Gln227, His226	Zn301
5b	-3.685	Gln227, His226	–
5c	-4.632	Tyr240	Zn301
5d	-4.953	–	Zn301
5e	-3.796	–	Zn301

Compound **5a** gave the most favourable Glide score (-5.900 kcal/mol) and interacted with Gln227, His226 and the catalytic Zn^{2+} center. Compounds **5b-e** occupied the MMP-9 binding region with different interaction patterns. Compounds **5d** and **5e** showed prominent interactions with Zn^{2+}, whereas **5c** gave a Glide score of -4.632 kcal/mol and interacted with Tyr240 and the catalytic Zn^{2+} center. The docked structures (Fig. 1) occupied the S1′ and S2′ regions, with the planar phthalimide nucleus providing an aromatic and hydrophobic surface and the anhydride carbonyl groups positioned toward the catalytic metal center. Zn^{2+} coordination and hydrophobic interactions within the substrate-binding region are recognized features of MMP inhibitor binding [11,12,16,26].

The detailed docking geometry of compound **5c** provided a basis for examining its proposed metal-binding mode. The distance between anhydride carbonyl oxygen O10 and Zn^{2+} was 2.31 Å. The Zn^{2+}–His226 NE2 and Zn^{2+}–His230 NE2 distances were 2.09 and 2.12 Å, respectively, while the reported Zn^{2+}–Glu402 OE1 distance was 2.18 Å. The Zn^{2+}–O10–C11 angle was 121.4º, close to the approximately 120º angle expected for the proposed local coordination geometry. The 2.31 Å Zn^{2+}–O10 distance is compatible with a Zn^{2+}–oxygen coordination interaction reported for zinc-containing metalloprotein systems [11,12,16,27]. These calculations support the placement of the anhydride carbonyl oxygen close to the catalytic Zn^{2+} center, although docking alone cannot establish the coordination mode experimentally.

The docking rank did not parallel the cellular cytotoxicity profile. Compound **5a** showed the most favourable docking score, whereas compound **5c** exhibited the lowest IC_{50} in the MTT assay. This difference is consistent with the contribution of physico-chemical properties, cellular uptake, intracellular distribution, metabolism and interactions with additional cellular targets to the biological response. The phenyl substituent of compound **5c** increases the aromatic surface and hydrophobic character of the molecule and may contribute to its cellular activity through enhanced hydrophobic and π-mediated interactions. Similar contributions of aromatic and hydrophobic groups have been reported in the design of MMP-directed compounds [28,29].

Molecular dynamics simulation: The dynamic behaviour of the **5c**–MMP-9 complex was investigated by a 100 ns

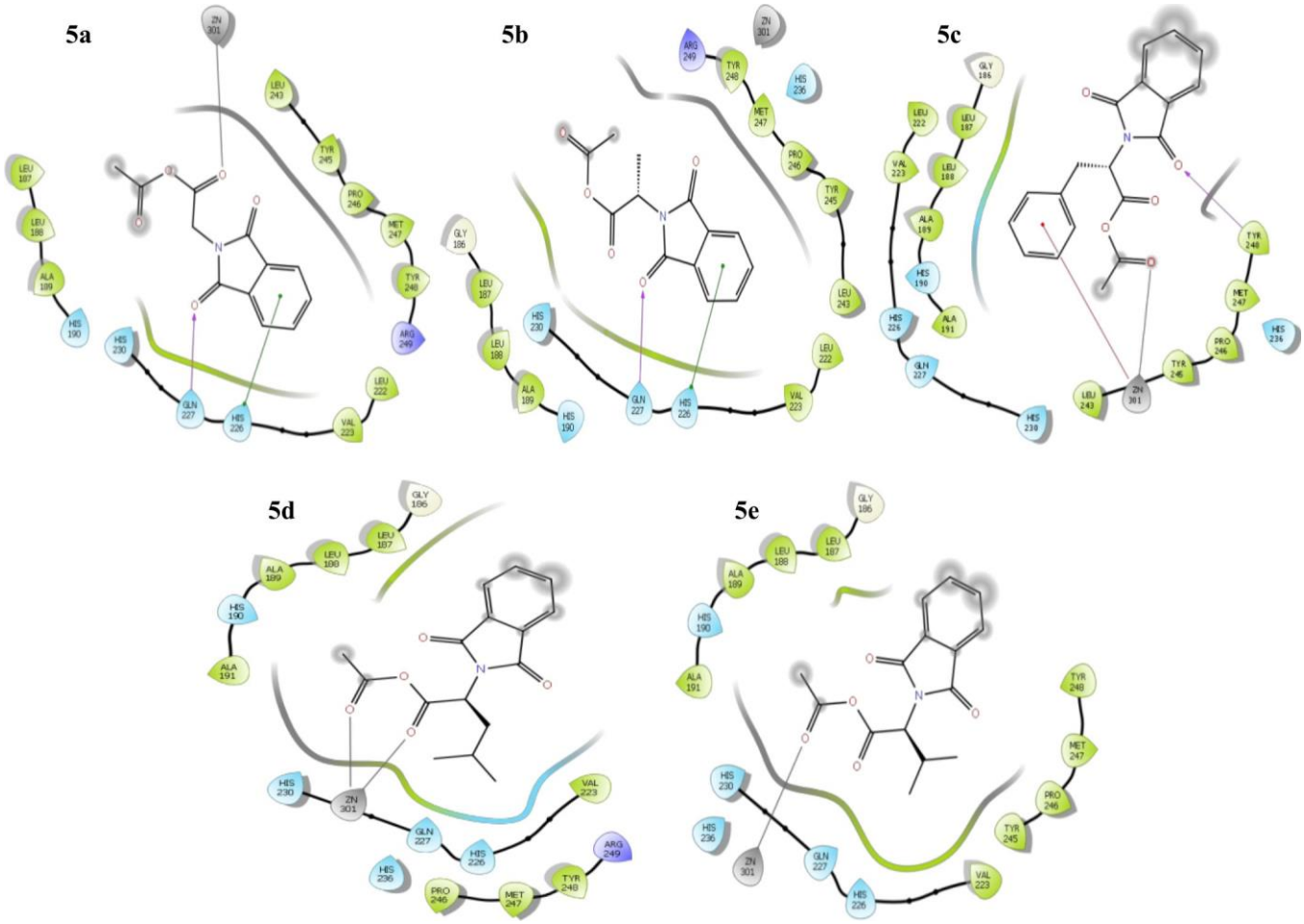

Fig. 1. Molecular docking poses of novel phthalimide-acyl anhydride derivatives (**5a-e**)

molecular dynamics simulation using the Desmond package. Compound **5c** was selected due to its favorable docking score (-4.632 kcal/mol) and cytotoxic activity against MCF-7 cells (IC_{50} = 27.89 μg/mL; 82.7 μM). The complex was simulated under NPT conditions at 300 K and 1.01325 bar after solvation in an SPC water environment and neutralization with counterions. Temperature and pressure regulation were performed using the Nose-Hoover chain thermostat and Martyna-Tobias-Klein barostat, respectively [20].

The RMSD profile (Fig. 2a) reached a relatively stable region after approximately 20 ns. Protein backbone and ligand RMSD values remained mainly within 1.5-2.5 Å during the simulation, which support the retention of the ligand within the MMP-9 binding region. RMSF analysis (Fig. 2b) showed limited fluctuations around the active site, with the lowest reported fluctuations reaching approximately 0.4224 Å. Gly112 and Asp113 exhibited higher fluctuations of 2.96 and 1.52 Å, respectively, consistent with higher local flexibility outside the principal ligand-binding region.

The protein–ligand interaction profile (Fig. 2c-d) has identified 24 interacting residues during the trajectory. The Tyr160, Tyr179, Phe181, Asp185, His226, Gln227, His230, His236 and Tyr248 contributed to the interaction network. Hydrogen bonds having Ala191, Gln227 and Leu188 showed occupancies of 92%, 48% and 84%, respectively. The π–π interactions having His230 and His236 showed occupancies of 77% and 31%, respectively. The anhydride group remained positioned near the catalytic Zn^{2+} center during the trajectory. The persistence of hydrogen-bonding, aromatic, hydrophobic and metal-site interactions supports the stability of the predicted compound **5c** binding orientation. Comparable interactions involving hydrophobic residues and aromatic contacts have been reported for MMP-9 inhibitor complexes [28,29]. The MD results support the docking model but do not establish experimental binding affinity or direct catalytic inhibition.

ADMET prediction: The pharmacokinetic and toxicity-related properties of compounds **5a-e** were predicted using SwissADME. All derivatives complied with Lipinski's rule of five and were predicted to possess high gastrointestinal absorption. None of the compounds was predicted to be a P-glycoprotein substrate and the computational models did not predict AMES mutagenicity or hERG inhibition. These characteristics provide a favourable preliminary drug-likeness profile and supported selection of the compounds for *in vitro* evaluation (Table-2). The predicted ADMET profile should be considered a computational screening result rather than experimental evidence of oral bioavailability or safety. This distinction is important for compound **5c**, since its subsequent acute oral toxicity study revealed a narrow safety margin.

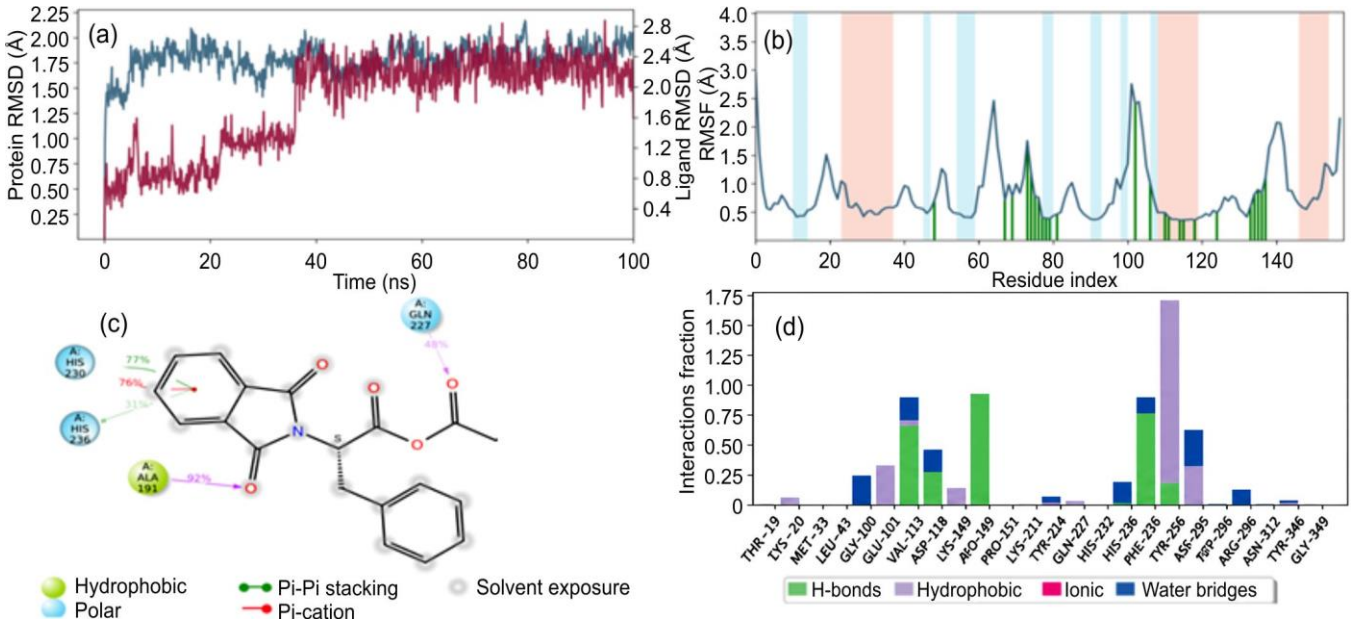

Fig. 2. Molecular simulation data of MMP-acetic 2-(1,3-dioxo-1,3-dihydro-2*H*-isoindol-2-yl)-3-phenylpropanoic anhydride (**5c**): (a) RMSD (protein RMSD is shown in grey while RMSD of compound **5c** are shown in red), (b) protein (MMP-9) RMSF, (c) 2D interaction diagram and (d) protein–ligand contact analysis of MD trajectory

TABLE-2
ADMET PARAMETERS OF SYNTHESIZED DERIVATIVES (**5a-e**)

Compound	Lipinski rule	GI absorption	BBB permeable	CYP_{450} inhibition	AMES toxicity	hERG inhibition
5a	Yes	High	No	None	No	No
5b	Yes	High	No	None	No	No
5c	Yes	High	No	None	No	No
5d	Yes	High	No	None	No	No
5e	Yes	High	No	None	No	No

Acute oral toxicity: Acute oral toxicity of compound **5c** was evaluated in female albino Wistar rats according to OECD Test Guideline 423, the Acute Toxic Class method [25]. At 300 mg/kg, all three animals developed lethargy and reduced activity and died within 48 h. At 50 mg/kg, two of three animals developed lethargy and died, while one animal survived without significant clinical signs. At 5 mg/kg, no lethargy or mortality was observed and all three animals survived the 14-day observation period. Based on the observed mortality pattern, the LD_{50} cut-off was assigned to the 5-50 mg/kg range, corresponding to GHS Category 2 under the OECD classification scheme.

The toxicity profile represents an important limitation for further development of compound **5c**. The favourable predicted ADMET characteristics were not accompanied by a broad experimental oral safety margin. The observed toxicity cannot be assigned to a specific structural feature without dedicated mechanistic studies. Possible contributions from anhydride hydrolysis, metabolic transformation, off-target interactions or inhibition of other MMP isoforms require investigation. MMP-2 and MMP-14, among other MMPs, have important roles in tumor biology and should be considered in subsequent selectivity studies [30]. Modification of the anhydride functionality, control of systemic exposure and tumour-directed delivery represent possible approaches for improving the therapeutic window [31].

***In vitro* evaluation**

Cytotoxicity by MTT assay: The cytotoxicity of compounds **5a-e** was evaluated against MCF-7 human breast cancer cells using the MTT assay. 5-Fluorouracil (5-FU), with an IC_{50} of 8.6 μg/mL (66.1 μM) under the conditions of the present study, was used as the reference compound. The synthesized derivatives were tested at 12.5, 25, 50 and 100 μg/mL for 24 h (Fig. 3). Compound **5c** exhibited the highest cytotoxic potency within the series, with an IC_{50} of 27.89 μg/mL (82.7 μM), followed by compound **5d** with an IC_{50} of 28.50 μg/mL (94.0 μM). Compounds **5a** and **5e** showed IC_{50} values of 34.78 μg/mL (140.7 μM) and 44.0 μg/mL (152.1 μM), respectively, while 5b was the least active derivative, with an IC_{50} of 177.13 μg/mL (678.2 μM) (Table-3). On a mass-concentration basis, compound **5c** had an IC_{50} approximately 3.2-fold higher than 5-FU (27.89 *versus* 8.6 μg/mL). On a molar basis, the corresponding values were 82.7 and 66.1 μM. Compound **5c** was therefore less potent than 5-FU under the present assay conditions, but it was the most active compound among the synthesized derivatives.

The phenyl substituent in compound **5c** increases aromatic surface area and lipophilicity and provides additional scope for π-mediated interactions. These properties may contribute to cellular uptake and interaction with hydrophobic biological sites. The branched aliphatic substituent in com-

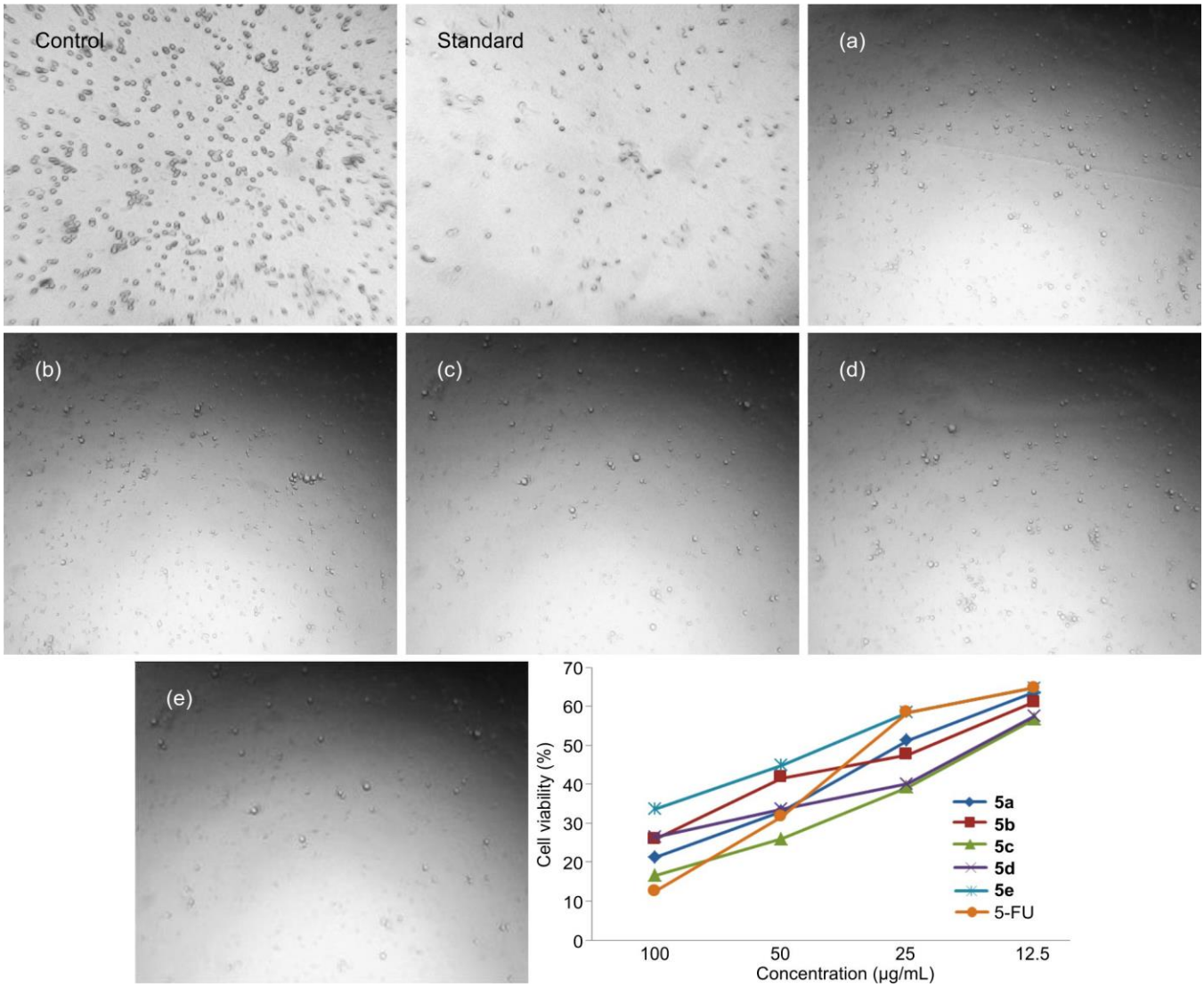

Fig. 3. MTT assay images and % cell viability of substituted acetic 2-(1,3-dioxo-1,3-dihydro-2*H*-isoindol-2-yl) anhydride derivatives (**5a-e**)

TABLE-3
CYTOTOXIC EFFECTS OF THE SYNTHESIZED COMPOUNDS ON MCF-7 CELLS DETERMINED BY THE MTT ASSAY AFTER 24 h

Compound	Concentration range (µg/mL)	% Cell viability (Mean ± SD)	IC_{50} (µg/mL)	IC_{50} (µM)	Activity level*
5a	100-12.5	21.08 ± 2.1–63.57 ± 1.8	34.78	140.7	Moderate
5b	100-12.5	25.78 ± 2.5–61.02 ± 2.0	177.13	678.2	Poor
5c	100-12.5	16.42 ± 1.9–56.66 ± 1.6	27.89	82.7	Fair
5d	100-12.5	26.41 ± 2.0–57.49 ± 1.7	28.50	94.0	Fair
5e	100-12.5	33.51 ± 1.9–64.69 ± 1.5	44.0	152.1	Moderate
5-FU (Std.)	100-12.5	12.41 ± 1.6–55.28 ± 1.2	8.6	66.1	Reference

*Activity level is expressed relative to 5-FU

pound **5d** produced a similar cytotoxic response, suggesting that both aromaticity and hydrophobic branching can influence activity within this series. The lower activity of compound **5b** indicates that the smaller methyl substituent does not provide the same contribution to cellular activity. The reported structure–activity studies of phthalimide and aromatic MMP-directed compounds support the importance of hydrophobic and aromatic substituent effects in molecular recognition [2,28,29].

Apoptosis induction: The mechanism associated with the cytotoxic activity of compound **5c** was examined using Annexin V-AbFluor™ 488/PI flow cytometry. Treatment of MCF-7 cells with compound **5c** at 30 µg/mL (88.93 µM) for 24 h increased the early apoptotic population from 9.3% in the control to 30.6%. Late apoptotic and necrotic populations were 0.8% and 1.25%, respectively. Cell viability decreased from 90.7% in the control to 67.4% after treatment with compound **5c** (Fig. 4). An increase in early apoptotic cells, toge-

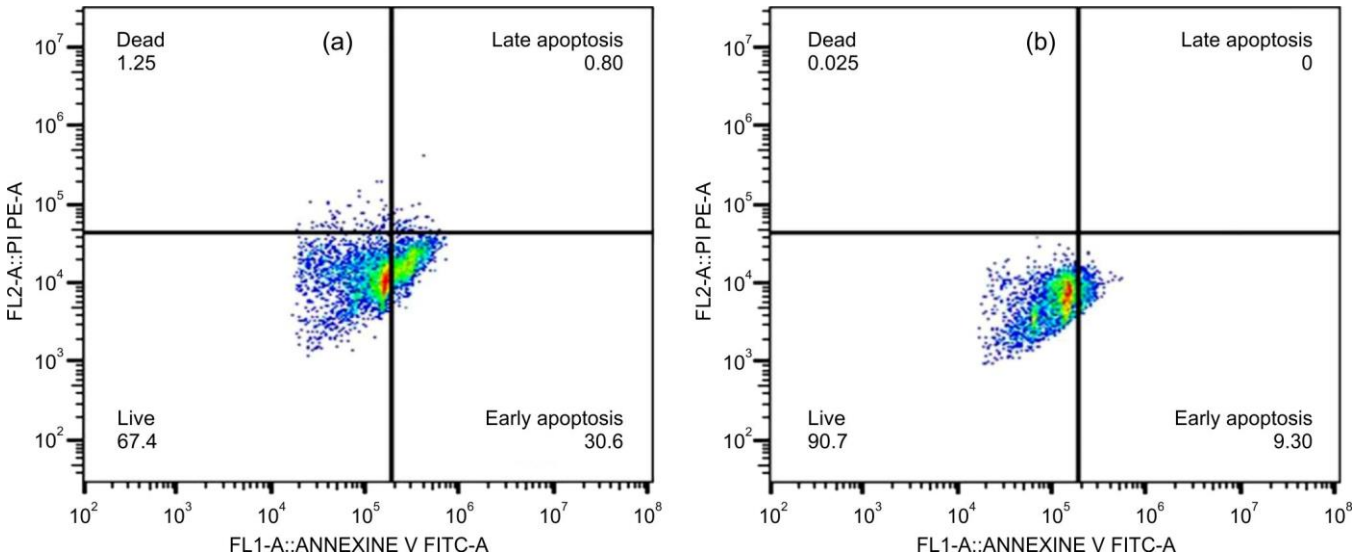

Fig. 4. Apoptosis study of compound **5c** by flow-cytometer: (a) negative control, (b) treated with compound **5c**

ther with the relatively small necrotic population, supports apoptosis as an important component of the cytotoxic response to compound **5c**. This observation is consistent with the role of apoptosis as a cellular response associated with anticancer activity of MMP-directed compounds [32].

Suppression of TPA-induced MMP-9 secretion: The effect of compound **5c** on TPA-induced MMP-9 secretion in MCF-7 cells was evaluated using the GENLISA™ Human MMP-9 ELISA kit. Compound **5c** was tested at ½IC_{50} (13.94 μg/mL; 41.3 μM), IC_{50} (27.89 μg/mL; 82.7 μM) and 2×IC_{50} (55.89 μg/mL; 165.7 μM), with 5-FU used as the reference compound (Table-4). TPA treatment was used to induce MMP-9 secretion, while untreated cells served as the basal control.

Treatment with compound **5c** produced a concentration-dependent decrease in MMP-9 levels. The reductions relative to the TPA-treated control were 24.75% at ½IC_{50}, 52.48% at IC_{50} and 64.36% at 2×IC_{50}. The concentration-dependent response provides cellular evidence that compound **5c** suppresses TPA-induced MMP-9 secretion. This finding is relevant to the proposed anticancer application since MMP-9 contributes to extracellular matrix degradation and processes associated with tumor invasion and metastasis [26,33].

The ELISA result should be interpreted specifically as suppression of MMP-9 secretion or extracellular MMP-9 levels, rather than direct enzymatic inhibition. Reduced MMP-9 levels may arise from altered transcription, secretion, cellular signaling or changes in viable cell number. The docking and MD results provide a structural basis for interaction of compound **5c** with the MMP-9 catalytic region, but they do not establish direct inhibition of the enzyme. A fluorogenic MMP-9 substrate assay using purified enzyme would be required to determine the direct inhibitory potency of compound **5c**. Selectivity testing against MMP-1, MMP-2, MMP-3 and MMP-14 would further establish whether the compound preferentially targets MMP-9.

The morphological changes observed in **5c**-treated MCF-7 cells (Fig. 5), together with the Annexin V/PI results, are consistent with the cytotoxic and apoptosis-associated response observed in the MTT assay. The combined cellular data support further investigation of compound **5c** as an MMP-9 associated anticancer hit, while the mechanistic relationship between MMP-9 suppression and apoptosis remains to be established experimentally.

Structure–activity relationship and lead assessment: The phthalimide nucleus provides a rigid aromatic framework, while the anhydride group introduces a carbonyl-rich region capable of positioning an oxygen atom near the catalytic Zn^{2+} center. Substitution derived from the amino acid component altered both the physico-chemical properties and cellular response of the compounds. The phenylalanine-derived **5c** gave the highest synthetic yield among the final derivatives (65%) and displayed the most favourable cellular cytotoxicity within the series.

TABLE-4
DOSE-DEPENDENT INHIBITION OF MMP-9 EXPRESSION BY COMPOUND **5c** IN MCF-7 CELLS USING ELISA

Compounds	Concentration (μg/mL)	Concentration (μM)	OD1	OD2	Mean OD	Calculated conc. (ng/mL)	Inhibition (%)
5c-1	13.94	41.3	0.068	0.051	0.0595	0.076	24.75
5c-2	27.89	82.7	0.054	0.051	0.0525	0.048	52.48
5c-3	55.89	165.7	0.048	0.050	0.0490	0.036	64.36
5-FU-1	0.650	5	0.051	0.053	0.0520	0.048	52.48
5-FU-2	1.3008	10	0.050	0.050	0.0470	0.040	60.40
5-FU-3	2.6016	20	0.048	0.046	0.0500	0.028	72.28
TPA	–	0.1	0.065	0.065	0.0650	0.101	0.00

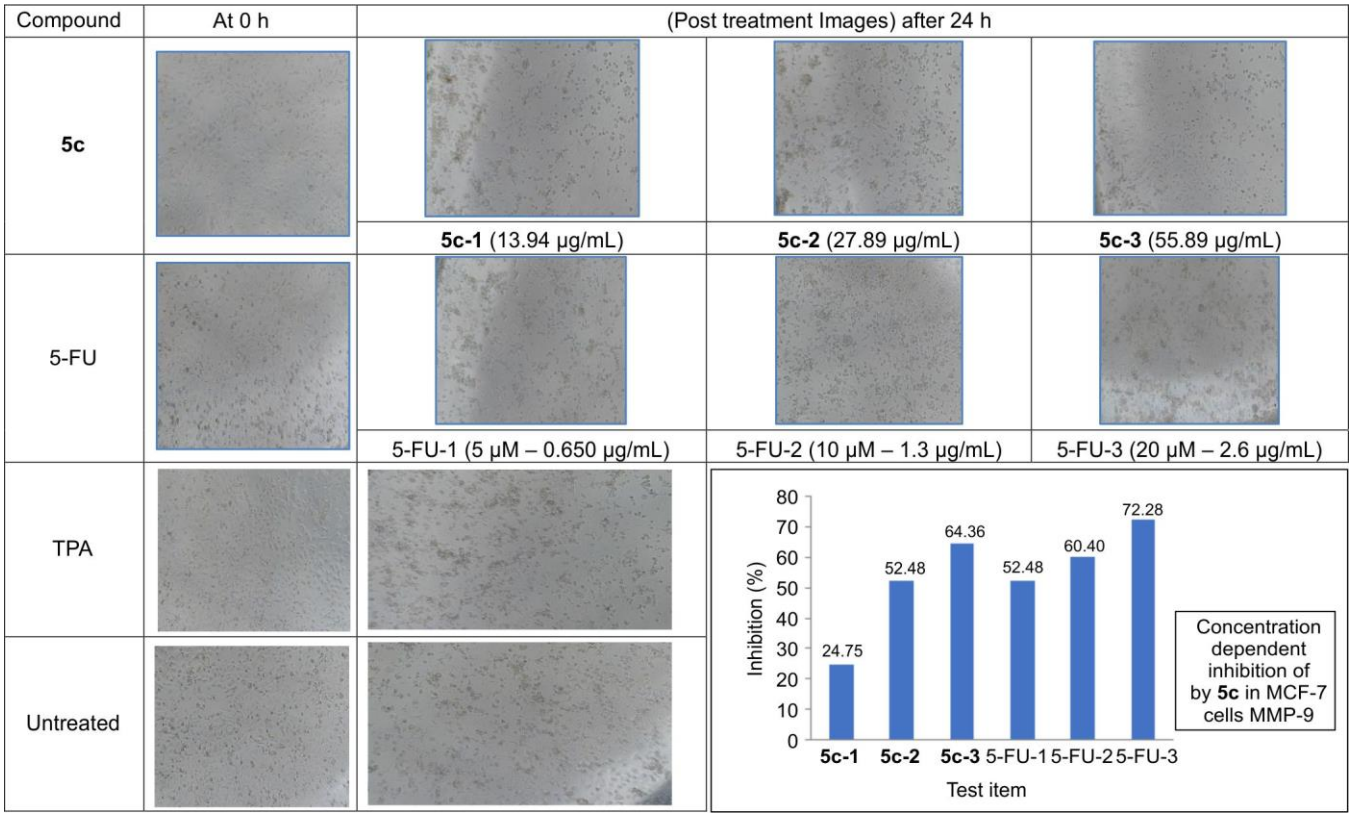

Fig. 5. Representative phase-contrast images of MCF-7 cells treated with compound **5c** and 5-FU at 0 and 24 h

Compound **5c** combined a Glide score of -4.632 kcal/mol with a stable 100 ns MD trajectory, predicted favourable drug-like properties, an MTT IC_{50} of 27.89 µg/mL (82.7 µM), increased early apoptosis and concentration-dependent suppression of TPA-induced MMP-9 secretion. The strong docking score of compound **5a** (-5.900 kcal/mol) compared with the higher cellular activity of compound **5c** illustrates the difference between predicted target affinity and cellular pharmacology. The phenyl group of **5c** may contribute to membrane association, hydrophobic recognition and π-mediated interactions, providing a possible explanation for its cellular activity.

The acute oral toxicity result is the principal limitation of compound **5c**. An LD_{50} cut-off of 5-50 mg/kg places the compound in GHS Category 2 and indicates a narrow experimental safety margin. The compound should consequently be regarded as a lead hit rather than a preclinical candidate at its present stage. The present findings establish the phthalimide-anhydride framework as a structurally distinct chemotype for MMP-9-targeted investigation.

Conclusion

The present study establishes phthalimide-conjugated acyl anhydrides (**5a-e**) as a promising chemotype for MMP-9 targeted breast cancer research. Among the synthesized derivatives, **5c** emerged as the lead hit, with a Glide score of -4.632 kcal/mol, stable MMP-9 binding during the 100 ns MD simulation (RMSD 1.5-2.5 Å) and cytotoxic activity against MCF-7 cells (IC_{50} = 27.89 µg/mL; 82.7 µM). Compound **5c** increased early apoptosis to 30.6% and reduced TPA-induced MMP-9 secretion by 64.36% at 55.89 µg/mL (165.7 µM). The phthalimide–anhydride framework provides a structurally distinct Zn^{2+}-binding motif that warrants further investigation as an alternative to conventional hydroxamate-based MMP inhibitor scaffolds. The acute oral toxicity profile remains a major limitation, with an LD_{50} cut-off of 5-50 mg/kg (GHS Category 2). Compound **5c** should presently be regarded as a lead hit rather than a preclinical candidate. Structure-toxicity optimisation is required to improve its therapeutic window while retaining MMP-9-associated activity. Direct enzymatic studies using recombinant human MMP-9, MMP-2 and MMP-1 are required to establish inhibitory potency and isoform selectivity. Further mechanistic studies, pharmacokinetic evaluation and *in vivo* efficacy and safety assessment will define the therapeutic potential of compound **5c** and guide development of optimized phthalimide–anhydride analogues for breast cancer research.

ACKNOWLEDGEMENTS

The authors acknowledge the funding received from Rajiv Gandhi Science and Technology Commission (RGSTC) Research Scheme, facilitated by Rashtrasant Tukadoji Maharaj Nagpur University, Nagpur, India [RTMNU/DIIL/2025/1300; Dated: 27 March, 2025].

CONFLICT OF INTEREST

The authors declare that there is no conflict of interests regarding the publication of this article.

DECLARATION OF AI-ASSISTED TECHNOLOGIES

During the preparation of this manuscript, the authors used an AI-assisted tool(s) to improve the language and no data, results or scientific conclusions were generated by AI. All analyses, interpretations and conclusions are the authors' own. The authors reviewed and edited the content and take full responsibility for the published work.

REFERENCES

1. U. Sharma, P. Kumar, N. Kumar and B. Singh, *Mini Rev. Med. Chem.*, **10**, 678 (2010); https://doi.org/10.2174/138955710791572442
2. M.L. Almeida, M.C.V.A. Oliveira, I.R. Pitta and M.G.R. Pitta, *Curr. Org. Syn.*, **17**, 252 (2020); https://doi.org/10.2174/1570179417666200325124712
3. H. Jiang and H. Li, *BMC Cancer*, **21**, 149 (2021); https://doi.org/10.1186/s12885-021-07860-2
4. Q. Wu, Z. Yang, Y. Nie, Y. Shi and D. Fan, *Cancer Lett.*, **347**, 159 (2014); https://doi.org/10.1016/j.canlet.2014.03.013
5. K. Kessenbrock, V. Plaks and Z. Werb, *Cell*, **141**, 52 (2010); https://doi.org/10.1016/j.cell.2010.03.015
6. S. Quintero-Fabián, R. Arreola, E. Becerril-Villanueva, J.C. Torres-Romero, V. Arana-Argáez, J. Lara-Riegos, M.A. Ramírez-Camacho and M.E. Alvarez-Sánchez, *Front. Oncol.*, **9**, 1370 (2019); https://doi.org/10.3389/fonc.2019.01370
7. M. Whittaker, C.D. Floyd, P. Brown and A.J.H. Gearing, *Chem. Rev.*, **99**, 2735 (1999); https://doi.org/10.1021/cr9804543
8. J.W. Skiles, N.C. Gonnella and A.Y. Jeng, *Curr. Med. Chem.*, **11**, 2911 (2004); https://doi.org/10.2174/0929867043364018
9. D.T. Puerta, M.O. Griffin, J.A. Lewis, D. Romero-Perez, R. Garcia, F.J. Villarreal and S.M. Cohen, *J. Biol. Inorg. Chem.*, **11**, 131 (2006); https://doi.org/10.1007/s00775-005-0053-x
10. S.K. Baidya, S. Banerjee, N. Adhikari and T. Jha, *J. Med. Chem.*, **65**, 10709 (2022); https://doi.org/10.1021/acs.jmedchem.1c01855
11. D.T. Puerta and S.M. Cohen, *Inorg. Chem.*, **41**, 5075 (2002); https://doi.org/10.1021/ic0204272
12. J.M. Zapico, L. Acosta, M. Pastor, L. Rangasamy, L. Marquez-Cantudo, C. Coderch, I. Ortin, M. Nicolau-Sanus, L. Puchades-Carrasco, P. Ramos, A. Pineda-Lucena, A. Majali-Martinez, B. de Pascual-Teresa and A. Ramos, *Int. J. Mol. Sci.*, **22**, 9976 (2021); https://doi.org/10.3390/ijms22189976
13. S.W. Khan, H.U. Rashid, S. Nayab, Husna, M. Khan and L. Rasheed, *Comput. Biol. Chem.*, **119**, 108565 (2025); https://doi.org/10.1016/j.compbiolchem.2025.108565
14. A. Kazakova, I. Frydrych, N. Jakubcová, J. Pokorný, B. Lišková, S. Gurská, R. Buriánová, A. Přibylka, P. Džubák, M. Hajdúch and M. Urban, *Eur. J. Med. Chem.*, **283**, 117126 (2025); https://doi.org/10.1016/j.ejmech.2024.117126
15. G.M. Sastry, M. Adzhigirey, T. Day, R. Annabhimoju and W. Sherman, *J. Comput. Aided Mol. Des.*, **27**, 221 (2013); https://doi.org/10.1007/s10822-013-9644-8
16. A. Tochowicz, K. Maskos, R. Huber, R. Oltenfreiter, V. Dive, A. Yiotakis, M. Zanda, T. Pourmotabbed, W. Bode and P. Goettig, *J. Mol. Biol.*, **371**, 989 (2007); https://doi.org/10.1016/j.jmb.2007.05.068
17. J.C. Shelley, A. Cholleti, L.L. Frye, J.R. Greenwood, M.T. Timlin and S. Uchimaya, *J. Comput. Aided Mol. Des.*, **21**, 681 (2007); https://doi.org/10.1007/s10822-007-9133-z
18. W. Sherman, H.S. Beard and R. Farid, *Chem. Biol. Drug Des.*, **67**, 83 (2006); https://doi.org/10.1111/j.1747-0285.2005.00327.x
19. Schrödinger, LLC, Maestro User Manual 2021. New York, NY, USA: Schrödinger, LLC (2021).
20. G.J. Martyna, D.J. Tobias and M.L. Klein, *J. Chem. Phys.*, **101**, 4177 (1994); https://doi.org/10.1063/1.467468
21. A. Daina, O. Michielin and V. Zoete, *Sci. Rep.*, **7**, 42717 (2017); https://doi.org/10.1038/srep42717
22. T. Mosmann, *J. Immunol. Methods*, **65**, 55 (1983); https://doi.org/10.1016/0022-1759(83)90303-4
23. I. Vermes, C. Haanen, H. Steffens-Nakken and C. Reutellingsperger, *J. Immunol. Methods*, **184**, 39 (1995); https://doi.org/10.1016/0022-1759(95)00072-I
24. Krishgen Biosystems, GENLISA™ Human MMP-9 ELISA Kit. User Manual Ver. 6.3. Mumbai: Krishgen (2023).
25. OECD, Test No. 423: Acute Oral Toxicity - Acute Toxic Class Method. OECD Guidelines for the Testing of Chemicals, Section 4. Paris: OECD Publishing (2002).
26. C.F. Adhipandito, D.P.K.S. Ludji, E. Aprilianto, R.I. Jenie, B. Al-Najjar and M. Hariono, *Future J. Pharm. Sci.*, **5**, 1 (2019); https://doi.org/10.1186/s43094-019-0001-1
27. B. Tamames, S.F. Sousa, J. Tamames, P.A. Fernandes and M.J. Ramos, *Proteins*, **69**, 466 (2007); https://doi.org/10.1002/prot.21536
28. T.P. Spicer, J. Jiang, A.B. Taylor, J.Y. Choi, P.J. Hart, W.R. Roush, G.B. Fields, P.S. Hodder and D. Minond, *J. Med. Chem.*, **57**, 9598 (2014); https://doi.org/10.1021/jm501284e
29. J.A. Jacobsen, J.L. Major Jourden, M.T. Miller and S.M. Cohen, *Biochim. Biophys. Acta Mol. Cell Res.*, **1803**, 72 (2010); https://doi.org/10.1016/j.bbamcr.2009.08.006
30. E.P.K. Conlon, M.W.P. O'Reilly and R.M. O'Connor, *J. Pathol.*, **247**, 508 (2019); https://doi.org/10.1002/path.5225
31. M.J. Fray and R.P. Dickinson, *Bioorg. Med. Chem. Lett.*, **11**, 571 (2001); https://doi.org/10.1016/S0960-894X(00)00720-4
32. J. Wang, Q. Li and X. Zhang, *J. Biomol. Struct. Dyn.*, **37**, 1234 (2019); https://doi.org/10.1080/07391102.2018.1455248
33. C.-J. Lee, T.-Y. Jang, S.-E. Jeon, H.-J. Yun, Y.-H. Cho, D.-Y. Lim and J.-S. Nam, *Nat. Commun.*, **15**, 10422 (2024); https://doi.org/10.1038/s41467-024-54920-9